Inorg. Chem. **2008**, *47*, 8604−8606

Coordination-Tuned Single-Molecule-Magnet Behavior of $Tb^{III}-Cu^{II}$ Dinuclear Systems

Takashi Kajiwara,*,† Motohiro Nakano,*,‡ Shinya Takaishi,† and Masahiro Yamashita†

Department of Chemistry, Graduate School of Science, Tohoku University, and CREST, Japan Science and Technology Agency (JST), Aramaki, Aoba-ku, Sendai 980-8578, Japan, and Department of Applied Chemistry, Graduate School of Engineering, Osaka University, Suita, Osaka 565-0871, Japan

Received July 21, 2008

$Tb^{III}-Cu^{II}$-based single-molecule magnet (SMM) and non-SMM were synthesized to investigate the relationship between magnetic anisotropy and the symmetry of the ligand field by the reaction of [TbCu(*o*-vanilate)$_2$(NO$_3$)$_3$] with methoxypropylamine ($MeOC_3H_6NH_2$, **1**) or ethoxyethylamine ($EtOC_2H_4NH_2$, **2**). In both complexes, Tb^{III} ions have a bicapped square-antiprism coordination geometry. When the Tb^{III} ion is in a less symmetrical ligand field, it has an easy-axis anisotropy and shows SMM behavior, whereas when it is in a more symmetrical environment, it has an easy-plane anisotropy and exhibits non-SMM behavior.

Single-molecule magnets (SMMs),[1−3] which show magnetic properties not observed previously, such as quantum spin tunneling, are chemically and physically fascinating compounds. The origin of the SMM behavior is the easy-axis magnetic anisotropy ($D < 0$), which causes the formation of an energy barrier that prevents reversal of the molecular magnetization and causes a slow relaxation of the magnetization at low temperature. SMMs form as a result of the combination of a large-spin multiplicity of the ground state and an easy-axis (or Ising-type) magnetic anisotropy of the entire molecule. Utilization of heavy lanthanide ions,[4−6] such as terbium(III) and dysprosium(III), has been one of the most elegant ways to design SMMs[4,5] because they have large angular momenta ($J = 6$ for Tb^{III} with $g_J = {}^3/_2$ and $J = {}^{15}/_2$ for Dy^{III} with $g_J = {}^4/_3$) in the ground multiplet state, which is derived from the strong spin−orbit coupling. Moreover, these metal ions are assumed to have a large Ising-type magnetic anisotropy.[4e,h,7] It is known that the symmetry of the ligand field around the lanthanide ion strongly affects the magnetic anisotropy,[8] and hence, it is worth studying how to control the magnetism of lanthanide-based SMMs via the symmetry of the ligand field. Here, we report a correlation between the symmetry of the ligand field and the magnetic anisotropy of $Tb^{III}-Cu^{II}$ dinuclear systems, in which a drastic switching from easy-axis to easy-plane anisotropy induced by a slight structural modification around the Tb^{III} ions, was observed.

Two new dinuclear Schiff base complexes, **1** and **2**, were synthesized from the dinuclear complex [TbCu(*o*-vanilate)$_2$(NO$_3$)$_3$][9] by reaction with methoxypropylamine ($MeOC_3H_6NH_2$) or ethoxyethylamine ($EtOC_2H_4NH_2$) (Figure 1).[10] In both complexes, two Schiff base ligands are arranged in a twisted manner around the Tb−Cu axis because of steric repulsion among the ligands' alkyl groups and weak coordination of the ether oxygens to the Cu^{II} ions. The degree of

* To whom correspondence should be addressed. E-mail: kajiwara@agnus.chem.tohoku.ac.jp (T.K.), moto@ch.wani.osaka-u.ac.jp (M.N.).
† Tohoku University.
‡ Osaka University.

(1) (a) Gatteschi, D.; Sessoli, R. *Angew. Chem., Int. Ed.* **2003**, *42*, 268. (b) Wernsdorfer, W.; Sessoli, R. *Science* **1999**, *284*, 133. (c) Aubin, S. M. J.; Sun, Z.; Pardi, L.; Krzystek, J.; Folting, K.; Brunel, L.-C.; Rheingold, A. L.; Christou, G.; Hendrickson, D. N. *Inorg. Chem.* **1999**, *38*, 5329. (d) Thomas, L.; Lionti, F.; Ballou, R.; Gatteschi, D.; Sessoli, R.; Barbara, B. *Nature* **1996**, *383*, 145.
(2) Blundell, S. J.; Pratt, F. L.; Lancaster, T.; Marshall, I. M.; Steer, C. A.; Hayes, W.; Sugano, T.; Letard, J.-F.; Caneschi, A.; Gatteschi, D.; Heath, S. L. *Phys. B* **2003**, *326*, 556.
(3) (a) Takeda, K.; Awaga, K.; Ohira, S.; Watanabe, I. *Synth. Met.* **2003**, *133−134*, 609. (b) Lascialfari, A.; Gatteschi, D.; Borsa, F.; Shastri, A.; Jang, Z. H.; Carretta, P. *Phys. Rev. B* **1998**, *57*, 514.
(4) (a) Osa, S.; Kido, T.; Matsumoto, N.; Re, N.; Pochaba, A.; Mronzinski, J. *J. Am. Chem. Soc.* **2004**, *126*, 420. (b) Zaleski, C. M.; Depperman, E. C.; Kampf, J. W.; Kirk, M. L.; Pecoraro, V. *Angew. Chem., Int. Ed.* **2004**, *43*, 3912. (c) Mishra, A.; Wernsdorfer, W.; Abboud, K. A.; Christou, G. *J. Am. Chem. Soc.* **2004**, *126*, 15648. (d) Aronica, C.; Pilet, G.; Chastanet, G.; Wernsdorfer, W.; Jacquot, J.-F.; Luneau, D. *Angew. Chem., Int. Ed.* **2006**, *45*, 4659. (e) Mori, F.; Nyui, T.; Ishida, T.; Nogami, T.; Choi, K.-Y.; Nojiri, H. *J. Am. Chem. Soc.* **2006**, *128*, 1440. (f) Costes, J.-P.; Dahan, F.; Wernsdorfer, W. *Inorg. Chem.* **2006**, *45*, 5. (g) Costes, J.-P.; Auchel, M.; Dahan, F.; Peyrou, V.; Shova, S.; Wernsdorfer, W. *Inorg. Chem.* **2006**, *45*, 1924. (h) Ueki, S.; Ishida, T.; Nogami, T.; Choi, K.-Y.; Nojiri, H. *Chem. Phys. Lett.* **2007**, *440*, 263. (i) Hamamatsu, T.; Yabe, K.; Towatari, M.; Matsumoto, N.; Re, N.; Pochaba, A.; Mrozinski, J. *Bull. Chem. Soc. Jpn.* **2007**, *80*, 523.
(5) (a) Ishikawa, N.; Sugita, M.; Ishikawa, T.; Koshihara, S.; Kaizu, Y. *J. Am. Chem. Soc.* **2003**, *125*, 8694. (b) Tang, J.; Hewitt, I.; Madhu, N. T.; Chastanet, G.; Wernsdorfer, W.; Anson, C. E.; Benelli, C.; Sessoli, R.; Powell, A. K. *Angew. Chem., Int. Ed.* **2006**, *45*, 1729.
(6) Chandrasekhar, V.; Pandian, B. M.; Azhakar, R.; Vittal, J. J.; Clérac, R. *Inorg. Chem.* **2007**, *46*, 5140.
(7) Schmitt, D. *J. Phys. (Paris)* **1986**, *47*, 677.
(8) Bleaney, B. *J. Magn. Reson.* **1972**, *8*, 91.
(9) Costes, J.-P.; Dahan, F.; Dupuis, A.; Laurent, J.-P. *Inorg. Chem.* **1997**, *36*, 3429.

10.1021/ic8013656 CCC: $40.75
Published on Web 08/29/2008

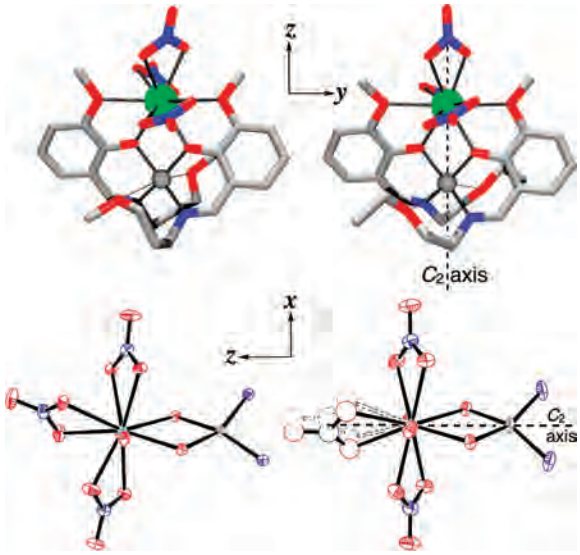

Figure 1. Top view of the molecular structures (upper) and side view of an ORTEP drawing of the cores (bottom) of the dinuclear complexes **1** (left) and **2** (right). Hydrogen atoms are omitted. In **2**, a nitrate ion is disordering around the 2-fold axis, which is depicted with solid and dashed curves. Color code: Tb, green; Cu, gray; O, red; N, blue; C, light gray.

twisting in **2** is slightly larger than that in **1**, with the dihedral angles between the O−Cu−N planes being 24.3(2)° in **1** and 26.7(2)° in **2**, and $O_{methoxy}$−Tb distances were 2.646(2) and 2.656(2) Å for **1** and 2.687(3) Å for **2**, which could be due to the smaller chelate rings in **2** than in **1**. In **2**, the larger twisting causes a longer $C_{methyl}\cdots C_{methyl}$ distance and relieves of the steric repulsion among two methoxy groups and a nitrate anion, leading to a more symmetrical coordination of the three nitrate ions than in **1**. As a result, in **2**, a nitrate anion and the Tb^{III} and Cu^{II} ions linearly align along the crystallographic 2-fold axis, and two axial nitrate ions are equivalent. The Tb^{III} ion in each complex has a bicapped square-antiprism coordination geometry, involving six nitrate oxygen atoms and two phenoxo oxygen atoms on the edges of the prism and two methoxy oxygen atoms, which cap the prism. **1** crystallized in the orthorhombic space group $Pna2_1$, and the crystallographic *a*, *b*, and *c* axes were aligned closely along the molecular $x - z$, *y*, and $x + z$ axes with deviations of 13°, 23°, and 24°, respectively (for more details, see Figure S1 in the Supporting Information). **2** crystallized in the monoclinic space group *C*2/*c*, and the crystallographic 2-fold axis is assigned to be the molecular *z* axis.

Alternating current susceptibility measurement for powdered samples of **1** (Figure 2) showed frequency-dependent out-of-phase signals, which indicate the presence of slow magnetic relaxation of **1** at low temperatures. A Cole−Cole plot at 2.0 K showed an ideal semicircle shape, confirming

(10) Crystallographic data for **1**: orthorhombic, space group $Pna2_1$, a = 20.1736(14) Å, b = 13.6047(10) Å, c = 11.2873(8) Å, V = 3097.9(4) Å^3, T = 100 K, Z = 4, 27 780 reflections were observed, of which 9003 were independent, R1 = 0.0268 [$I > 2\sigma(I)$] and wR2 = 0.0453 (all data) for 419 parameters. Crystallographic data for **2**·2MeOH: monoclinic, space group *C*2/*c*, a = 18.875(2) Å, b = 12.5755(14) Å, c = 16.3540(18) Å, β = 116.640(2)°, V = 3469.8(7) Å^3, T = 100 K, Z = 4, 16 194 reflections were observed, of which 4937 were independent, R1 = 0.0436 [$I > 2\sigma(I)$] and wR2 = 0.1118 (all data) for 223 parameters.

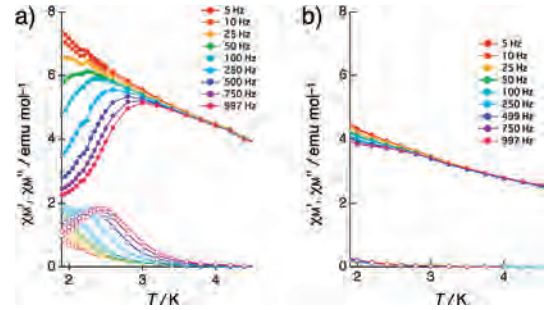

Figure 2. Temperature dependences of χ_M' (closed circles) and χ_M'' (open circles) of (a) **1** and (b) **2** measured with an 1000 Oe external direct current field.

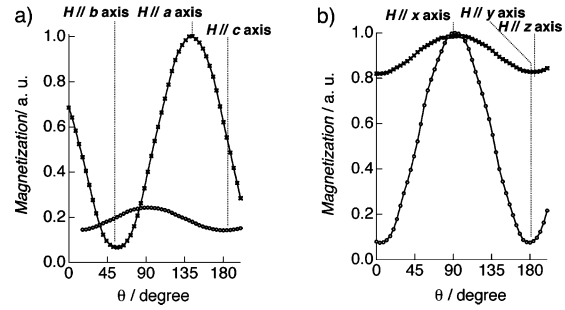

Figure 3. Angular dependence of the magnetization measured for single crystals rotating around the $a + b$ (○) and c (×) axes for (a) **1** and the y (×) and z (○) axes for (b) **2**. To avoid the influences of possible intermolecular magnetic interactions,[4g] the data were collected at 10 K.

that the relaxation process occurs via a single process, and the energy barrier, Δ/k_B, for the spin flipping in **1** was estimated from the Arrhenius plot to be 16.6(5) K (Figure S4 in the Supporting Information). On the other hand, **2** does not show SMM behavior even with an external magnetic field up to 1000 Oe, which prevents tunneling relaxation processes.

To reveal the differences in magnetic anisotropy in these complexes, magnetizations of single crystals of both complexes were investigated. Figure 3a shows a plot of the angular dependence of the normalized magnetization measured for **1** rotating around $a + b$ and *c* axes. One maximum along the *a* axis and two minima along the *b* and *c* axes were found, which shows the presence of an easy axis along the *a* axis, or molecular $x - z$ axis. For **2**, the angular dependence of the magnetization measured around the *y* and *z* axes (Figure 3b) shows one maximum along the *x* axis and two minima along the *z* and *y* axes with values of $1 \approx 0.85 \gg 0.1$, indicating that **2** has an easy-plane anisotropy in the *zx* plane.

The magnetic interactions were studied on the basis of the temperature dependence of $\chi_M T$ (Figure 4), which were measured for single crystals of **1** and **2** with a magnetic field applied along crystallographic *a* and *b* axes for **1** and along molecular *x* and *y* axes for **2**. $\chi_M T$ values were different for **1** and **2** at low temperatures. In the low-temperature region, the Tb^{III} ion with an f^8 configuration is populated only in the $^7F_6$ ground state of $|J,J_z\rangle = |6,J_z\rangle$ ($J_z = \pm 6, \pm 5, \ldots, 0$), whereas the Cu^{II} ion with a d^9 configuration has an $S = {}^1/_2$ spin. A superexchange interaction, J_{ex}, gives rise to 26

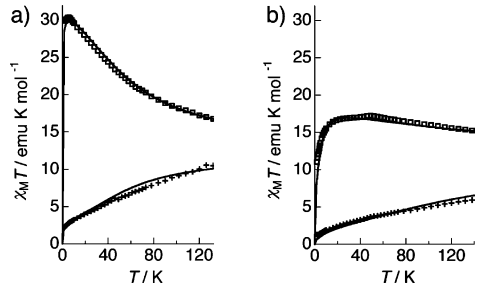

Figure 4. Temperature dependence of $\chi_M T$ values for single crystals of (a) **1** and (b) **2**. The magnetic field was applied along crystallographic *a* (□) and *b* (+) axes for **1** and along molecular *x* (□) and *y* (+) axes for **2**, respectively. Solid curves are the theoretical curves with the parameters described in the main text.

sublevels as a result. The temperature dependence of $\chi_M T$ was analyzed by using the following Hamiltonian:

$$\hat{\mathbf{H}} = -2J_{ex}\hat{\mathbf{J}}\cdot\hat{\mathbf{S}} + B_2^0\hat{\mathbf{O}}_2^0 + B_2^2\hat{\mathbf{O}}_2^2 - \beta\mathbf{H}\cdot(g_S\hat{\mathbf{S}} + g_J\hat{\mathbf{J}})$$

where **H** denotes the applied magnetic field, β is the Bohr magneton, B_2^0 and B_2^2 are second-order anisotropy parameters of the Tb^{III} ion, $\hat{\mathbf{O}}_2^0 = 3\hat{\mathbf{J}}_z^2 - \hat{\mathbf{J}}^2$ and $\hat{\mathbf{O}}_2^2 = (\hat{\mathbf{J}}_+^2 + \hat{\mathbf{J}}_-^2)/2$, which are Stevens' operator equivalents[11] corresponding to axial and rhombic anisotropy, respectively. Usually higher-order anisotropy terms ($\hat{\mathbf{O}}_4^0$, $\hat{\mathbf{O}}_4^4$, $\hat{\mathbf{O}}_6^0$, etc.) should be included in magnetic analysis of rare-earth compounds;[12] however, it appeared that the magnetic susceptibilities of the present complexes were fortunately reproducible by considering only quadratic anisotropy terms, partly owing to the statistical property of thermodynamic quantities, which may smear out the fine structures of spin-energy levels. The observed $\chi_M T - T$ curves could be reproduced when J_{ex}/k_B, B_2^0/k_B, and B_2^2/k_B were assumed to be +3, −1.8, and −0.1 K for **1** and 3, 3.2, and 0.1 K for **2**, respectively. In both complexes, weak ferromagnetic interactions between the Cu^{II} and Tb^{III} ions occur to give large-spin ground states. The difference in the $\chi_M T - T$ curves of the two compounds is mainly due to the difference in the B_2^0 values, which again is indicative of the easy-axis anisotropy of Tb^{III} in **1** and the easy-plane anisotropy in **2**.

The difference in the magnetic anisotropies of **1** and **2** is attributed to the slightly different morphology of the ligand field originating from a slightly different arrangement of nitrate ligands around the Tb^{III} ions. Figure 5 shows the negative charge distributions around Tb^{III} ions that were obtained from density functional theory (DFT) calculations. The f-electron distribution corresponding to the $J_z = \pm 6$ states has an oblate spheroidal profile,[7] and the accompanying magnetic momentum is parallel to the flattening axis *z* with L_z values of ±3. On the other hand, the main components of $|6,0\rangle$ are $|0,0\rangle_{LS}$ and $|\pm 1,\mp 1\rangle_{LS}$ ($|S_z,L_z\rangle_{LS}$ denotes a

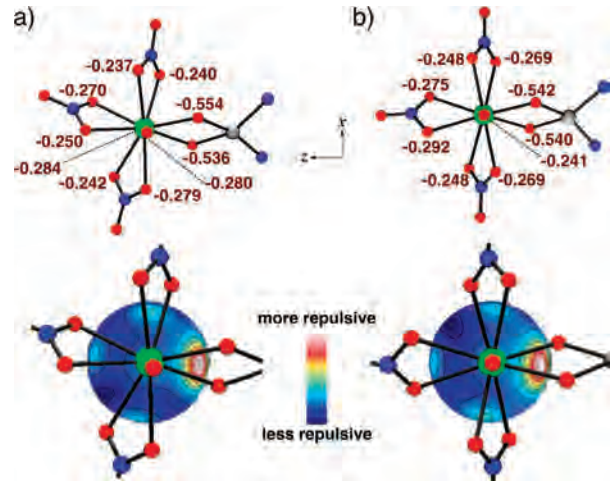

Figure 5. (top) Mulliken charges of donating oxygen atoms and (bottom) electrostatic potentials on the spheres with a radius of 1.5 Å from the Tb^{3+} ion for (a) **1** and (b) **2**, respectively. The results were obtained from DFT calculations performed for the atomic coordinates from X-ray structural analysis.

corresponding LS vector), which have a prolate spheroidal electron distribution. In **1**, less repulsive areas were found in the second and fourth quadrands, and oblate-shaped $|6,\pm 6\rangle$ electronic clouds could be stabilized in this area with the easy-axis directing along the $x-z$ direction. In **2**, the electronic distributions on the first and fourth quadrands are equivalent because of the 2-fold axis passing through the Tb−Cu axis, and hence the Tb^{III} ion is surrounded by negative charges in a symmetrical manner around the molecular *zx* plane, and a prolate-shaped $|6,0\rangle$ electronic cloud might be located with the principal axis directing along the *y* axis.

In conclusion, we showed the importance of the symmetry of the ligand field in $Tb^{III}-Cu^{II}$ dinuclear systems, which affects the magnetic anisotropy of the Tb^{III} ions and causes a drastic change from easy-axis to easy-plane anisotropy. These results provide a useful guideline for the design of the magnetic anisotropy of lanthanide ions, yielding novel SMM and single-chain magnet families based on highly anisotropic lanthanide ions.

Acknowledgment. This work was supported by a Grant-in Aid for Scientific Research of Priority Areas "Panoscopic Assembling and High Ordered Functions for Rare Earth Materials" from the Ministry of Education, Culture, Science, Sports, and Technology, Japan.

Supporting Information Available: Experimental procedure for the preparation of the complexes, detail of X-ray crystallographic analyses, and magnetic data (PDF) and X-ray crystallographic file (CIF). This material is available free of charge via the Internet at http://pubs.acs.org.

IC8013656

(11) Stevens, K. W. H. *Proc. Phys. Soc. London* **1952**, *A65*, 209.
(12) *Crystal Field Handbook*; Newman, D. J., Ng, B. K. C., Eds.; Cambridge University Press: Cambridge, U.K., 2000.